Collisional deactivation of vibrationally highly excited azulene in compressed liquids and supercritical fluids

D. Schwarzer, J. Troe, M. Votsmeier, and M. Zerezke

Citation: The Journal of Chemical Physics **105**, 3121 (1996); doi: 10.1063/1.472180
View online: http://dx.doi.org/10.1063/1.472180
View Table of Contents: http://scitation.aip.org/content/aip/journal/jcp/105/8?ver=pdfcov
Published by the AIP Publishing

Collisional deactivation of vibrationally highly excited azulene in compressed liquids and supercritical fluids

D. Schwarzer, J. Troe, M. Votsmeier, and M. Zerezke
Max-Planck-Institut für Biophysikalische Chemie, Am Fassberg, D-37077 Göttingen, Germany

(Received 26 March 1996; accepted 14 May 1996)

The collisional deactivation of vibrationally highly excited azulene was studied from the gas to the compressed liquid phase. Employing supercritical fluids like He, Xe, CO_2, and ethane at pressures of 6–4000 bar and temperatures $\geqslant$380 K, measurements over the complete gas–liquid transition were performed. Azulene with an energy of 18 000 cm^{-1} was generated by laser excitation into the S_1 and internal conversion to the S_0^*-ground state. The subsequent loss of vibrational energy was monitored by transient absorption at the red edge of the $S_3 \leftarrow S_0$ absorption band near 290 nm. Transient signals were converted into energy-time profiles using hot band absorption coefficients from shock wave experiments for calibration and accounting for solvent shifts of the spectra. Under all conditions, the decays were monoexponential. At densities below 1 mol/l, collisional deactivation rates increased linearly with fluid density. Average energies $\langle \Delta E \rangle$ transferred per collision agreed with data from dilute gas phase experiments. For Xe, CO_2, and C_2H_6, the linear relation between cooling rate and diffusion coefficient scaled collision frequencies Z_D turned over to a much weaker dependence at $Z_D > 0.3$ ps^{-1}. Up to collision frequencies of $Z_D = 15$ ps^{-1} this behavior can well be rationalized by a model employing an effective collision frequency related to the finite lifetime of collision complexes. © *1996 American Institute of Physics.*
[S0021-9606(96)01232-9]

I. INTRODUCTION

Collisional energy transfer from vibrationally highly excited polyatomic molecules to bath gas molecules has been extensively studied over the last decade.[1,2] In most cases, hot molecules were prepared by light absorption into electronically excited states which undergo fast internal conversion to the electronic ground state. The subsequent decay of vibrational energy was monitored by time resolved uv absorption,[3–5] ir emission,[6,7] energy-selective photoionization,[8] or by other techniques leading to ''energy loss profiles,'' from which values of the product $\langle \Delta E \rangle Z$ were derived directly. $\langle \Delta E \rangle$ denotes the average energy transferred per collision and Z is the reference number of collisions per time.[9] The dependence of $\langle \Delta E \rangle$ on the average internal energy $\langle E \rangle$ of the molecule, the nature of the excited molecule, the bath gas, and the temperature was investigated. Though not all details of the observed vibrational energy transfer in the gas phase are understood, considerable progress towards its quantitative characterization could be achieved.[10–13]

In contrast to the gas phase, studies of collisional energy transfer of vibrationally highly excited polyatomic molecules in liquid solvents have been much less extensive (see Refs. 14–20 and review Ref. 21 with references cited therein). Since transient signals recorded during the collisional deactivation process usually were not calibrated unambiguously quantitative information about the product $\langle \Delta E \rangle Z$ is available only to a very limited extent. In particular, the applicability of isolated binary collision (IBC) concepts for describing collisional energy transfer of polyatomics in liquids was neither proved nor disproved. In this approach one quantifies the complex solute–solvent interaction by gas phase like binary collisions and one assumes that the solvent density affects only the collision frequency, but not the mechanism of vibrational relaxation. The predictions of this model then depend on the somewhat arbitrary definition of an appropriate collision frequency.

We have shown previously[22–24] that isomerization and atom recombination rate constants scale with the inverse of the solvent self-diffusion coefficient D over the gas–liquid phase transition, suggesting that effective collision frequencies Z increase proportional with D^{-1}. Using D^{-1} scales for the density dependence of vibrational relaxation in liquids, i.e., for collisional energy transfer of only slightly excited molecules, has also been suggested on theoretical grounds.[25] The question arises whether this scaling can also be used for collisional energy transfer of highly excited polyatomic molecules. It, therefore, appears highly desirable to study collisional energy transfer over wide density ranges, from low pressure gases up into compressed liquids. Using supercritical solvents, measurements over continuous density ranges can be performed without gaps at gas–liquid phase transitions.

In the present work, vibrationally highly excited azulene, formed by light absorption into the S_1 state and subsequent internal conversion to the ground state, served as a model system. The internal conversion rate ($k_{ic} = 1.0$ ps^{-1} [26]) is fast enough to allow for measurements of collisional energy transfer even in liquids where this process occurs on the 10 ps time scale. In contrast to earlier work,[16,18] where transient absorption signals were obtained at the red edge of the $S_1 \leftarrow S_0$ absorption band near 720 nm, we followed the loss of vibrational energy at the red edge of the $S_3 \leftarrow S_0$ band near 290 nm. This has several advantages:

(i) The energy dependence of the ground state absorption

spectrum of gaseous azulene near 290 nm is well characterized by shock wave and laser excitation experiments up to internal excess energies of 35 000 cm^{-1}.[27]

(ii) The difference between molar absorption coefficients of ''hot'' and ''cold'' azulene is of the order of 10^4 $l\,mol^{-1}\,cm^{-1}$, giving rise to much larger absorption signals than at the red edge of the $S_1 \leftarrow S_0$ band where it is only 10^2 $l\,mol^{-1}\,cm^{-1}$.

(iii) The results can be compared directly with low pressure gas phase experiments where the collisional deactivation was also monitored near 290 nm.[5]

II. EXPERIMENTAL TECHNIQUE

In our experiments azulene was excited with light pulses near 600 nm and probed by light pulses near 300 nm. The required pulses were generated by a laser system employing a colliding pulse mode locked dye laser. Its output pulses at a wavelength of 620 nm were amplified in a three stage dye amplifier[28] which was pumped by a Nd:YAG laser (Continuum 6050) at a 50 Hz repetition rate. After recompression, the pulse width was less than 100 fs at an energy of ~140 μJ. 50% of the energy was used to generate a white light continuum in a 1 cm water cell. Using interference filters, a spectral band at twice the desired probe wavelength was amplified in two subsequent Rhodamine 6G dye cells and frequency doubled in a potassium dihydrogen phosphate (KDP) crystal. In this way probe pulses in the range 290–300 nm were generated. Pulses at fundamental wavelengths of 580–600 nm were used to pump azulene into its first excited singlet state. Excitation and probe energies were ~60 and 2 μJ, respectively. Both laser pulses were fed into a standard pump–probe interferometer, recombined, and collinearly focused into the sample cell. The relative plane of polarization was adjusted to 54.7° by means of a zeroth-order half-wave plate. Probe energies were determined in front of and behind the sample cell by means of photodiodes. Behind the sample, an interference filter for the respective probe wavelength was used to block transmitted excitation light. The time resolution of the experiment was limited mainly by the internal conversion rate of 1.0 ps^{-1} and not by the width of the cross correlation of both laser pulses of $\Delta\tau$=650 fs (FWHM) which was determined in separate experiments.

Measurements in liquids at 1 bar were performed in a 2 mm quartz flow cell. High-pressure experiments in liquids at pressures up to 4000 bar at room temperature were carried out in a stainless steel cell with sapphire windows, whose thickness and aperture were 2.5 and 2.0 mm, respectively. The optical path length inside the cell was 2 mm. This cell was connected to a high-pressure pump generating a flow through the sample cell which was fast enough to replace the irradiated sample volume between successive excitation pulses. Experiments in gases and supercritical fluids at pressures up to 1000 bar were performed in a heatable high pressure cell with an optical path length of 20 mm. Sapphire windows with a thickness of 10 mm and an aperture of 7 mm were used. Temperatures were determined with an accuracy of 1 K. In all pump–probe experiments, azulene concentrations were adjusted to an optical density of 1.0–1.5 at 290 nm (corresponding to 2 and 0.2 mM for optical path lengths of 2 and 20 mm, respectively) which, even for the lowest gas densities used in this work, was sufficient to avoid azulene–azulene collisions during the collisional deactivation process.

In order to monitor the collisional deactivation of azulene, we observed the changes of azulene absorption at the red edge of the $S_3 \leftarrow S_0$ transition after laser excitation. The temperature dependence of the azulene absorption band in this region was known from shock wave experiments in the range 800–1500 K.[27] In order to get additional information about the temperature dependence of the absorption at lower temperatures, we measured azulene absorption coefficients in a quartz cell with an optical path length of 5 cm in a Varian Cary 5E spectrometer. This cell was filled with a known amount of azulene dissolved in *n*-pentane, cooled down to 183 K, evacuated to remove solvent and air, and then sealed off by melting. In this way the concentration of azulene in the cell remained constant while heating up in the spectrometer. Formation of naphthalene by thermally activated isomerization could be neglected below ~600 K. Only at higher temperatures naphthalene was identified due to its strong absorption at 212 nm.

With increasing solvent density, the absorption spectrum of azulene shows a marked red shift due to electronic interactions with the bath gas. In molecular solvents like *n*-pentane at 1 bar, the shift of the $S_3 \leftarrow S_0$ band is on the order of 10 nm. Since the temperature dependence of the azulene absorption coefficient was found to depend critically on the wavelength,[27] the solvent shift of the spectrum had to be taken into account in the conversion of the transient signals into energy-time profiles. For this purpose, we had to assume that, for a given bath gas, the solvent shift of azulene spectra was temperature independent and could be characterized by the density-dependent redshift of the room temperature spectrum. Redshifts $\Delta\lambda$ of the room temperature spectra as a function of solvent density were measured separately in a high pressure cell with an optical path length of 10 mm. It was shown in Refs. 5, 27, and 29 that ''canonically hot spectra'' of thermally excited azulene and ''microcanonically hot spectra'' from laser excited azulene are identical when ensembles of the same average energy are compared. We had to assume that this is true as well in dense fluids as in low pressure gases.

Azulene (Merck >98% pure), high purity solvents (J. T. Baker, p.a. grade) and gases (Messer–Griesheim) were used without further purification.

III. RESULTS

A. Excitation dependence and solvent shift of azulene spectra

The temperature dependence of steady state absorption spectra of gaseous azulene is illustrated in Fig. 1, comparing our present results with earlier results from shock wave experiments.[27] The absorption coefficients obtained from our thermal spectra are used to calibrate transient absorption sig-

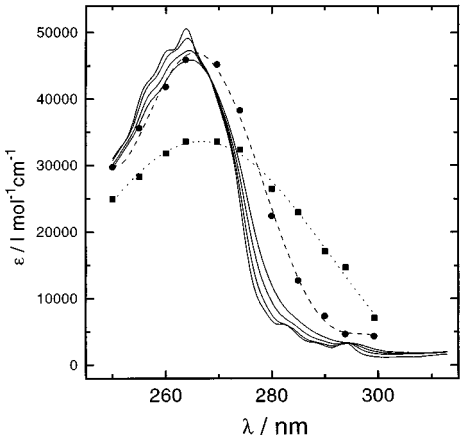

FIG. 1. Absorption coefficients of azulene in the gas phase [full lines: 323, 398, 478, and 564 K, static cell, from this work; (●) 800 K, (■) 1500 K, shock wave experiments (Ref. 27)].

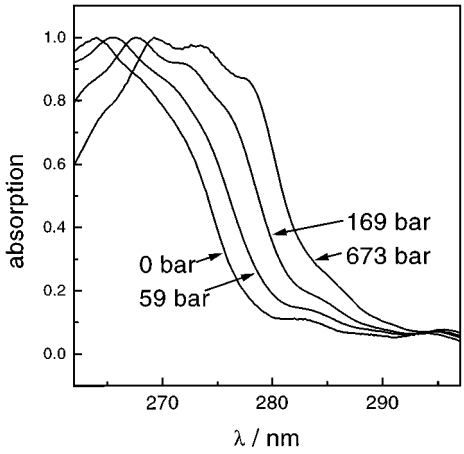

FIG. 3. Pressure dependence of absorption spectra of azulene in C_2H_6 at 385 K.

nals from collisional energy transfer studies. For this purpose, the molar decadic absorption coefficient ϵ of azulene in Fig. 2 is plotted against the average energy $\langle E\rangle$ of azulene for several fixed wavelengths. Average energies $\langle E\rangle$ were calculated for the temperatures shown in Fig. 1 with azulene vibrational frequencies from Ref. 30. The results of this work agree perfectly with our earlier results.[27] Polynomial fits of $\epsilon\langle E\rangle$ in the range 1 000–19 000 cm^{-1} lead to

$$\epsilon_{280}(\langle E\rangle)/\mathrm{l\,mol^{-1}\,cm^{-1}} = 616.6 + 3.844(\langle E\rangle/\mathrm{cm^{-1}}) - 1.819\cdot 10^{-4}(\langle E\rangle/\mathrm{cm^{-1}})^2 + 3.052\cdot 10^{-9}(\langle E\rangle/\mathrm{cm^{-1}})^3, \quad (1)$$

$$\epsilon_{290}(\langle E\rangle)/\mathrm{l\,mol^{-1}\,cm^{-1}} = 2362 + 0.5297(\langle E\rangle/\mathrm{cm^{-1}}), \quad (2)$$

$$\epsilon_{300}(\langle E\rangle)/\mathrm{l\,mol^{-1}\,cm^{-1}} = 1166 + 0.2091(\langle E\rangle/\mathrm{cm^{-1}}). \quad (3)$$

At wavelengths 290 and 300 nm, ϵ depends linearly on $\langle E\rangle$, i.e., transient absorption signals obtained at these wavelengths during the collisional deactivation of azulene directly reflect the loss of vibrational energy as a function of time. However, this is valid only at low densities. At higher densities, one has to take into account the solvent shift of the azulene absorption spectrum. As a consequence of solvent–solute electronic interactions, the absorption spectrum shifts to the red such as shown in Fig. 3 for several pressures of the bath gas ethane at 384 K. The redshift of the S_3 band becomes more pronounced with increasing density; at liquid densities, it amounts to about 10 nm (see Fig. 4).

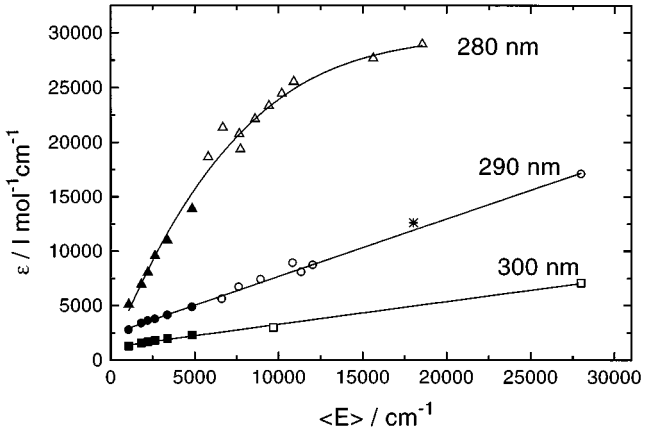

FIG. 2. Energy dependence of azulene absorption coefficient in the gas phase at selected wavelengths [filled symbols: from this work; open symbols: from shock wave experiments (Ref. 27); (*) from laser excitation experiments (Ref. 27)].

B. Collisional energy transfer

1. $\langle \Delta E\rangle$ values in the gas phase

At first we present signals recorded at low gas densities where a solvent shift of the spectra is negligible. Since under these conditions the ''solubility'' of azulene in the bath gas

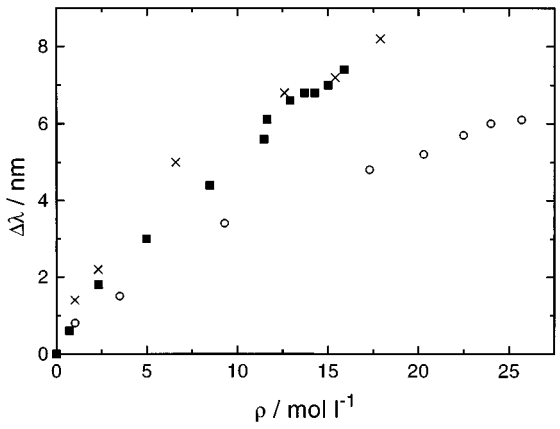

FIG. 4. Solvent shift of the azulene S_3 absorption band in Xe (×), CO_2 (○), and C_2H_6 (■).

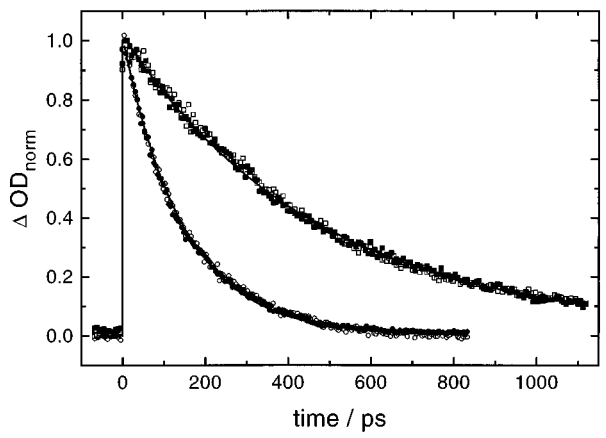

FIG. 5. Absorption-time profiles recorded during the collisional deactivation of azulene in C_2H_6 at 384 K (□: 6.25 bar, λ_{pr}=300 nm; ■: 6.25 bar, λ_{pr}=290 nm; ○: 21.25 bar, λ_{pr}=300 nm; ●: 21.25 bar, λ_{pr}=290 nm; full lines: monoexponential fits).

is very low, experiments were performed at 380–445 K to increase the azulene vapor pressure and the absorption signals. Because of the linear dependence between ϵ and $\langle E\rangle$ [see Eqs. (2) and (3)], probing hot azulene at wavelengths 290 and 300 nm directly monitors the loss of vibrational energy with time and, therefore, signals at different wavelengths should be of similar shape. This is indeed the case, such as shown in Fig. 5 for azulene in C_2H_6 at bath gas pressures of 6.25 and 21.25 bar at $T\approx$384 K. The maximum change of the optical density at 290 nm is ~0.3 and a factor of 2.5 less at 300 nm; this is in accord with Fig. 2. The energy-loss profiles $\langle E(t)\rangle$ presented in Fig. 5 are monoexponential, i.e.,

$$\langle E(t)\rangle=\langle E_0\rangle\exp(-t/\tau_c) \quad \text{for } t>0, \tag{4}$$

such as indicated by solid lines; $\langle E_0\rangle$ denotes the photon energy of the excitation pulse and τ_c is a phenomenological cooling time constant. Average values for τ_c in C_2H_6 at 6.25 and 21.25 bar of 445 and 139 ps, respectively were obtained; i.e., within experimental error the cooling rate was found to increase proportional to pressure, following simple gas phase behavior. This dependence was observed for all investigated bath gases at $T\geqslant$380 K and pressures below ~30 bar.

Numerical simulations of the master equation for collisional deactivation of vibrationally highly excited molecular states have shown[9] that the slope of the energy-loss curves $\langle E(t)\rangle$ directly lead to average energies $\langle\Delta E\rangle$ transferred per collision through

$$\frac{d\langle E\rangle}{dt}=Z\cdot\langle\Delta E\rangle \tag{5}$$

as long as the energy dependence of $\langle\Delta E\rangle$ is not too strong and the distribution of excited molecules is sufficiently far from the final thermal equilibrium. Combining Eqs. (4) and (5) gives

$$\langle\Delta E\rangle=-\langle E\rangle/(Z\cdot\tau_c). \tag{6}$$

TABLE I. Average energies $\langle\Delta E\rangle$ transferred per collision and comparison with dilute gas phase experiments.[a]

Gas	$-100\ m_{\langle\Delta E\rangle}$	$-\langle\Delta E\rangle_{15\,000\ \mathrm{cm}^{-1}}$ (cm^{-1}) This work	Ref. 5	Ref. 6	Ref. 8	$\tau_D^{-1}\cdot N_{\max}$ (ps^{-1}) [Eq. (16)]
He	0.40	60	80	45	50	65
Xe	0.63	95	170	125	105	1.8
N_2	0.70	105	180	145	120	7.5
CO_2	1.51	227	360	333	210	2.4
C_2H_6	2.54	380	430			3.9

[a]Calculated with Lennard-Jones collision frequencies from Ref. 31.

For an exponentially decaying $\langle E(t)\rangle$ curve, one concludes that $\langle\Delta E\rangle$ linearly depends on $\langle E\rangle$ with slope of

$$m_{\langle\Delta E\rangle}=-1/(Z\cdot\tau_c). \tag{7}$$

Identifying Z with the Lennard-Jones collision frequency Z_{LJ} and using Lennard-Jones parameters σ=6.61 Å and ϵ/k_B=523 K for azulene and values as tabulated in Ref. 31 for the collision partners, one obtains $m_{\langle\Delta E\rangle}$ for He, Xe, N_2, CO_2, and C_2H_6 such as summarized in Table I.

2. Evaluation of energy-loss profiles at higher densities

The transient uv absorption signals recorded during the collisional deactivation not all decay monoexponentially. This is shown in Fig. 6 for room temperature transients observed in Xe at liquid densities and at a probe wavelength of λ_{pr}=290 nm. After excitation, the decay of the signals accelerates for the first 100–200 ps and only afterwards turns over to a more or less exponential decay. This behavior becomes more pronounced at higher Xe pressures; it is caused by the increasing redshift of the absorption spectrum which amounts to 10 nm at 2040 bar Xe. At this pressure, the signal recorded at 290 nm essentially corresponds to low pressure gas phase signals recorded at 280 nm; i.e., instead of $\epsilon_{290}(\langle E\rangle)$ from Eq. (2) one has to use $\epsilon_{280}(\langle E\rangle)$ from Eq. (1)

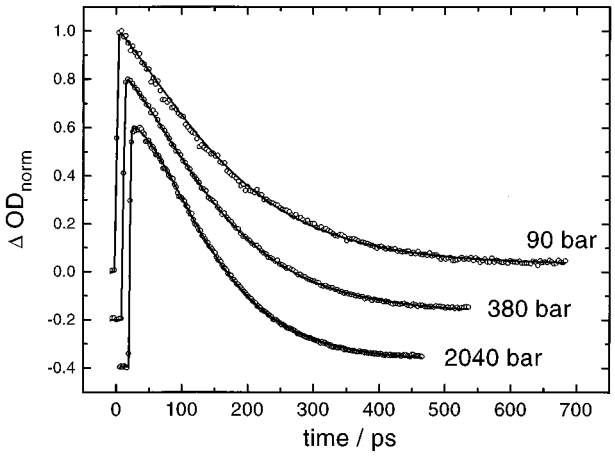

FIG. 6. As Fig. 5, in Xe at 295 K and various pressures (λ_{pr}=290 nm; full lines: fits using the model function of Eq. (10); time origins have been shifted for clarity).

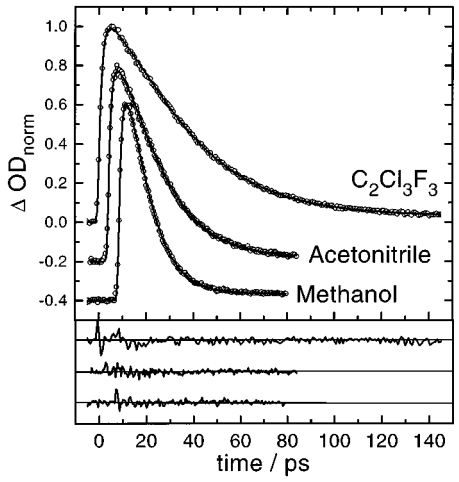

FIG. 7. As Fig. 5, in liquid solvents at 1 bar, $T=296$ K ($\lambda_{pr}=290$ nm; full lines: fits using the model function of Eq. (10); time origins have been shifted for clarity).

TABLE II. Vibrational deactivation times τ_c of azulene in various solvents at 1 bar and 296 K.

Solvent	Probe wavelength λ_{pr} (nm)	Solvent shift $\Delta\lambda$ (nm)	τ_c (ps)
n-pentane	290	8	12.5
n-heptane	290	8.5	13.3
n-octane	290	9	11.8
n-decane	290	9	11.6
n-hexadecane	290	11	10.8
Cyclohexane	295	9	13
	291.5	9	13.7
	286.5	9	14.5
Acetonitrile	290	9	14.6
Methanol	290	8	8.3
Methanol-d_1	290	8	9.2
Methanol/water 1:3	290	8	3.3
Ethanol	290	9	9.0
Ethylenglycol	290	14	7.2
$C_2Cl_3F_3$	290	8	25.9

for calibration. The latter has a fairly weak energy dependence at $\langle E\rangle \geqslant 10\,000$ cm^{-1} which, in Fig. 6, results in relatively slow signal decays at early times. Similar shapes of the transients were observed in all liquid molecular solvents at 1 bar and 296 K when a probe wavelength of 290 nm was used. Representative signals for 1,1,2-tri-chloro-tri-fluoro-ethane, acetonitrile, and methanol are shown in Fig. 7. The following procedure was employed to model the data: Accounting for the redshift of the absorption spectrum, an effective gas phase probe wavelength $\lambda_{eff}=\lambda_{pr}-\Delta\lambda$ was defined. Then the energy dependence of the absorption coefficient $\epsilon_{\lambda\ eff}(\langle E\rangle)$ at λ_{eff} was evaluated from Eqs. (1)–(3) by interpolation and polynomial fitting. Assuming an exponential time dependence for $\langle E\rangle$, such as expressed by Eq. (4), leads to the time dependence of the absorption coefficient

$$\epsilon_{\lambda\ eff}(t)=\epsilon_{\lambda\ eff}(\langle E(t)\rangle+\langle E_c\rangle) \tag{8}$$

which is directly related to the transient absorption signal by

$$S^*(t)=A_0[\epsilon_{\lambda\ eff}(t)-\epsilon_{\lambda\ eff}(\langle E_c\rangle)]+s_0. \tag{9}$$

Here, $\langle E_c\rangle$ denotes the thermal equilibrium energy of azulene before laser excitation and A_0 is a scaling factor. In most cases a small residual absorption s_0 was observed at late times which remained constant for at least 1.5 ns. Finally the internal conversion process (time constant τ_{ic}) and a finite Gaussian shaped instrument response (time resolution $\Delta\tau=650$ fs) were taken into account by convolution of $S^*(t)$

$$S(t)=\int_0^\infty\int_0^{\tau'} S^*(\tau)\cdot\exp\left(-\frac{\tau'-\tau}{\tau_{ic}}\right)d\tau \times\exp\left(-4\ln 2\left(\frac{t-\tau'}{\Delta\tau}\right)^2\right)d\tau' \tag{10}$$

and fit to the data. The results for $S(t)$ are plotted as full lines in Figs. 5–7, using τ_c, τ_{ic}, A_0, and s_0 as fit parameters. On average, the time constant for internal conversion was found to be $\tau_{ic}=1.0$ ps which is in accord with the value reported in Ref. 26. The agreement between model and signals is excellent even though the time dependence of $\langle E\rangle$ *a priori* does not have to be exponential. However, fitting of the model function (10) to the data was satisfactory in all cases, such that no indication for a nonexponential decay of $\langle E\rangle$ during the collisional deactivation of azulene was found in any of our experiments.

3. Energy-loss time constants τ_c

Our results for τ_c are summarized in Tables II to VIII. Because of uncertainties in the calibration curves, systematic errors of τ_c on the order of 10% are estimated, the statistical error of τ_c being about 5% and 10% for signals recorded at 290 and 300 nm, respectively. In Table II, τ_c values for solvents at 1 bar are presented. In general, the vibrational deactivation in liquids under ambient conditions takes about 10 ps. Only in halogenated solvents the cooling time is remarkably longer ($\tau_c=25.9$ ps in $C_2Cl_3F_3$) which confirms earlier observations.[16,18] The high accuracy of our data allowed to establish the following trends: for *n*-alkanes, τ_c decreases with increasing chain length from 12.5 ps in *n*-pentane to 10.8 ps in *n*-hexadecane; hydrogen bond formation has a strong influence on the collisional deactivation rate: with increasing hydrogen bond density, τ_c decreases from ethanol (9.0 ps) to methanol (8.3 ps), ethylenglycol (7.2 ps) and a 3:1 mixture of water and methanol (3.3 ps). Deuteration of the OH group in methanol leads to an increase of τ_c by 10%. Compression of the liquids has only a minor influence on the collisional deactivation rate (see Table III), e.g., pressurizing *n*-octane from 1 to 4000 bar leads to a decrease of τ_c from 11.8 to 8.4 ps.

More insight into the pressure dependence of the collisional deactivation is obtained by investigating the process in supercritical solvents, thus avoiding the density discontinuity at the gas–liquid phase transition. The results of corresponding experiments are summarized in Table IV–VIII for He,

TABLE III. Vibrational deactivation times τ_c of azulene in compressed liquid solvents at 296 K (λ_{pr}=290 nm).

	p(bar)	$\Delta\lambda$(nm)	τ_c(ps)
n-pentane			
	1	8	12.5
	615	8.5	10.9
	1053	9	10.3
	2010	9.5	9.6
	3480	10	8.2
n-octane			
	1	9	11.8
	1575	10	10.1
	2800	10.5	8.9
	4000	11	8.4
CHF_3			
	65	5.5	21.2
	297	6	18.1
	1039	7	14.3
	1820	8	12.9
SF_6			
	37	5	17.4
	240	6	14.6
	696	7	12.7

N_2, Xe, CO_2, and C_2H_6. Figures 8–12 show plots of τ_c^{-1} vs the density for these solvents. Whereas in He and N_2 τ_c^{-1} increases nearly linearly with density, in Xe, CO_2, and C_2H_6 the initially linear increase of τ_c^{-1} becomes weaker near 1 mol/l. At very high densities (ρ>20 mol/l), where the packing density $n=\rho\sigma^3$ (with σ being the Lennard-Jones diameter of the solvent) approaches a value of 1, the slope of the density dependence of τ_c^{-1} becomes steeper again.

4. Effective collision frequencies in dense media

In the gas phase, the rate constant for collisional energy transfer τ_c^{-1} is proportional to the binary collision frequency Z. This quantity, of course, is not well defined under liquid phase conditions such that one may look for a replacement. We have shown earlier[22–24] that rate constants for isomerization and atom recombination under transport control scale with the inverse D^{-1} of the solvent self diffusion coefficient. D^{-1} therefore may be used as a measure of the effective collision frequency which, on the basis of the relation $Z\cdot D$ =const., was defined as

TABLE IV. Vibrational deactivation times τ_c of azulene in He.

p bar	T K	ρ mol l^-	D 10^{-9} m^2 s^{-1}	Z_D ps^{-1}	λ_{pr} nm	$\Delta\lambda$ nm	τ_c ps
23.2	383	0.726[a]	8550[b]	0.382	290	0	614
47	385	1.45	4290	0.761		0.5	302
81	386.5	2.46	2530	1.29		1	189
81		2.46	2530	1.29		1	192
152		4.52	1380	2.37		1.5	114
295		8.37	745	4.38		3	61
437		11.9	525	6.22		4	43
593	387.5	15.4	405	8.06		5	33

[a]Reference 32.
[b]Reference 33.

TABLE V. Vibrational deactivation times τ_c of azulene in Xe.

p bar	T K	ρ mol l^{-1}	D 10^{-9} m^2 s^{-1}	Z_D ps^{-1}	λ_{pr} nm	$\Delta\lambda$ nm	τ_c ps
16	382	0.532[a]	558[b]	0.153	290	0	1170
31	383	1.071	279	0.306		0.5	650
46	384	1.655	183	0.468		0.5	460
61		2.30	133	0.644		1	380
63		2.39	128	0.669		1	354
79		3.16	97.4	0.877		1.5	274
108		4.75	65.1	1.31		2	221
90	295	13.0	16.3	4.14		6	124
380		18.0	8.67	7.77		7	107
1026		21	5.37	12.6		8.5	94
2040		23.3	4.70	14.3		10	86
8	384	0.259	1150	0.075	300		2000
16		0.529	564	0.152			1020
30		1.03	291	0.294			550
45	385	1.61	188	0.454			390
45		1.61	188	0.456			400
60		2.25	136	0.628			340

[a]Reference 34.
[b]Reference 35.

$$Z=Z_D(p_2)=\frac{Z_{LJ}(p_1)\cdot D_g(p_1)}{D(p_2)}. \tag{11}$$

Here, Z_{LJ} and D_g correspond to the dilute gas phase, e.g., at p_1=1 mbar. Values for $D(p_2)$, used to calculate Z_D for high densities, are tabulated in Tables III–VIII. Figures 13–17 show plots of τ_c^{-1} vs Z_D. Except for He, where a nearly linear relation is observed over the entire pressure range, the dependence of τ_c^{-1} on Z_D for Xe, CO_2, and C_2H_6 is linear at low pressures, but becomes much weaker for Z_D>0.3 ps^{-1}. This change of behavior occurs at densities where Z_D is about a factor of 30 below liquid phase values.

IV. DISCUSSION

A. $\langle\Delta E\rangle$ values in the gas phase

The present work is completely consistent with earlier studies of collisional energy transfer of azulene in the dilute gas phase.[5,6,8] A comparison of $\langle\Delta E\rangle$ values at an excitation energy of E=15 000 cm^{-1} is included in Table I. The data from Ref. 5 which were obtained using basically the same experimental technique (by monitoring uv absorption changes at 290 nm) are systematically somewhat larger. The deviations from the results of Ref. 6, where $\langle\Delta E\rangle$ was deter-

TABLE VI. Vibrational deactivation times τ_c of azulene in N_2.

p bar	T K	ρ mol l^{-1}	D 10^{-9} m^2 s^{-1}	Z_D ps^{-1}	λ_{pr} nm	$\Delta\lambda$ nm	τ_c ps
57	384	1.76[a]	515[b]	0.657	290	1	203
60	407	1.74	540	0.684		1	230
61	424	1.69	570	0.648		1	221
123	428	3.28	290	1.27		2	142
194	424	5.04	179	2.06		3	92

[a]Reference 36.
[b]Reference 37.

TABLE VII. Vibrational deactivation times τ_c of azulene in CO_2.

p bar	T K	ρ mol l^{-1}	D 10^{-9} m^2 s^{-1}	Z_D ps^{-1}	λ_{pr} nm	$\Delta\lambda$ nm	τ_c ps
6.25	384	0.204[a]	2670[b]	0.075	290	0	900
11.25		0.371	1480	0.136		0	515
21.25	385.5	0.713	800[c]	0.251		0	270
40		1.403	413	0.487		0.5	154
43	383	1.53	382	0.526		0.5	142
74		2.86	215	0.935		0.5	97
107	384	4.56	136	1.48		1	73
147		7.00	89	2.27		1.5	57
149	386	7.00	89	2.27		1.5	59
151	384	7.26	85	2.36		1.5	52
202	385	10.3	56	3.59		2.5	44
247	387	12.1	41	4.92		2.5	42
359	386	15.6	18.3	11.0		3.5	33
694	387	19.8	7[d]	28.7		4.5	30
1163		22.6	5	39.4		5	27
1757		24.7	3	67.0		5.5	22
2207		25.9	2	100		6	21
11.3	442	0.319	1930[b]	0.119		0	535
21.5		0.61	1010[c]	0.226		0	295
32.5	445	0.93	670	0.341		0	213
50	447	1.47	430	0.534		0.5	152
83	444	2.5	271	0.848		0.5	108
87	296	17.3	10.3	15.2		4	30.1
1180		26.3	2.31	67.6		6	22.4
3080		29	1.5[d]	104		6.5	18.7
6.25	386.5	0.203	2700[b]	0.074	300		920
11.25		0.369	1500	0.134			485
21		0.712	815[c]	0.248			275
41		1.45	410	0.493			175
42	383	1.49	390	0.513			145
74		2.88	215	0.935			104
88	387	3.49	190	1.05			95
107	384	4.56	136	1.48			77
147		7.0	89	2.27			59
202	385	10.3	56	3.59			48
202		10.3	56	3.59			50

[a]Reference 38.
[b]Reference 37.
[c]Reference 33.
[d]Reference 39.

TABLE VIII. Vibrational deactivation times τ_c of azulene in C_2H_6.

p bar	T K	ρ mol l^{-1}	D 10^{-9} m^2 s^{-1}	Z_D ps^{-1}	λ_{pr} nm	$\Delta\lambda$ nm	τ_c ps
6.25	383	0.201[a]	2400[c]	0.098	290	0	450
11.25		0.367	1340	0.176		0	240
21.25	383.9	0.718	700	0.335		0.5	130
29	385	1.01	515	0.456		0.5	100
34	383	1.21	442	0.532		0.5	90
58.5	385.5	2.291	260	0.90		1	51
78		3.33	175[d]	1.36		1.5	37
79	386	3.32	175	1.35		1.5	36
102		4.82	113	2.08		2	29
118		5.83	90	2.61		2.5	25.3
118		5.83	90	2.61		2.5	25.1
131		6.61	77	3.06		3	23.6
170		8.45	55.5	4.23		3.5	20.0
249		10.55	40.1	5.86		4.5	17.1
251		10.58	39.9	5.89		4.5	17.4
360	385	12.1	31.8	7.39		5.5	15.3
583		13.8	25.0	9.4		6	13.5
1040	386	17[b]	15.3	15.4		7.5	12.2
55	296	11.8	26.6	6.90		5	15.9
498		15.9	13.8	13.3		7	12.4
1470		18.5	8.46	21.7		8	10.1
2110		19.6	6.6[e]	27.8		8.5	9.3
2975		20.7	4.95	37.1		9	8.3
3470		21.1	4.41	41.6	300	9.5	8.0
6.25	384	0.200[a]	2420[c]	0.097			430
21.25	385	0.715	710	0.329			148
78	383	3.39	169[d]	1.39			37.5
117	383	5.93	87.6	2.68			27.3
169	381	8.71	53	4.46			19.8
251	382	10.8	38.5	6.10			18.1
360		12.2	31.2	7.53			16.8
585		13.9	24.5	9.6			12.8
1062		17[b]	15.1	15.6			12.8

[a]Reference 40.
[b]Extrapolated from Ref. 40 following Ref. 41.
[c]Reference 37.
[d]Reference 42.
[e]Extrapolated from Ref. 42.

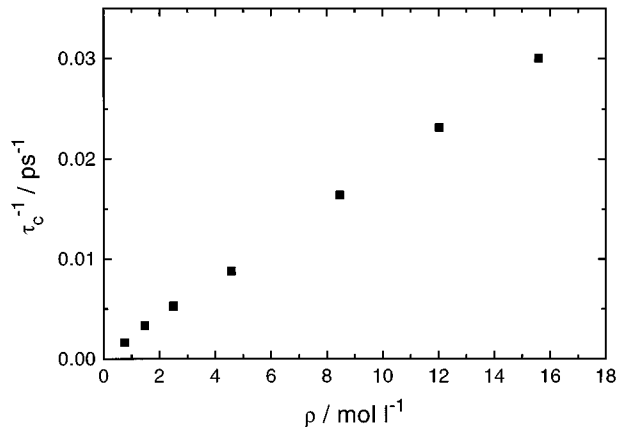

FIG. 8. Rate constants of the collisional deactivation of excited azulene in He.

mined by detecting ir fluorescence of azulene during the collisional deactivation, are smaller, but again (except for He) the values of this work seem to be systematically lower. However, recent $\langle \Delta E \rangle$ values from Ref. 8, determined using multiphoton ionization are in good agreement with the present data. Probably the discrepancies reflect the systematic uncertainties of the different experimental methods.

Average energies transferred per collision in Ref. 43 for the bath gases He and N_2 were determined at excitation energies as high as 53 000 cm^{-1} being 160 ± 40 cm^{-1} and 410 ± 70 cm^{-1}, respectively. A linear extrapolation of our data to this excitation energies gives 210 and 370 cm^{-1}, respectively, indicating that $\langle \Delta E(E) \rangle$ for He and N_2 increases nearly linearly even up to these high energies.

B. Collisional deactivation rates at densities >1 mol/l

The agreement of the absolute $\langle \Delta E \rangle$ values discussed so far implies that the mechanism of collisional energy transfer does not change from the dilute gas phase to astonishingly high densities in compressed gases, i.e., the concept of iso-

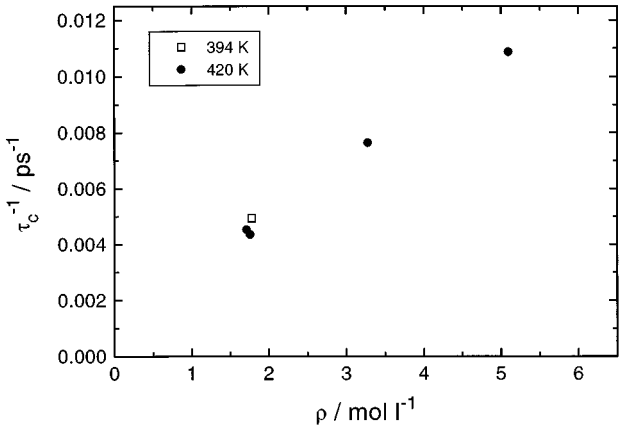

FIG. 9. As Fig. 8, bath gas N_2.

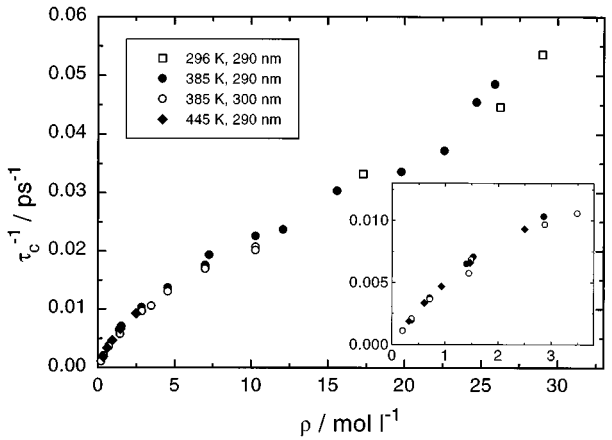

FIG. 11. As Fig. 8, bath gas CO_2.

lated binary collisions (IBC)[44] for He works well up to nearly the highest density used in this work (16 mol/l), whereas for N_2, Xe, CO_2, and C_2H_6 it works up to ~1 mol/l. For the latter bath gases the increase of τ_c^{-1} at higher pressures turns over into a weaker Z_D dependence. The extrapolation of collisional deactivation rates from the gas phase therefore, leads to much higher values than those actually observed in liquid solvents (see Tables II and III). The same behavior in our group was found for the collisional deactivation of cycloheptatriene[45] in compressed supercritical fluids and liquids which suggests that our present work reflects quite general behavior. In the following we discuss possible explanations for these properties of collisional energy transfer.

1. Local heating of the solvent

In the simple IBC model, a complete exchange of surrounding bath gas molecules between collisions with the vibrationally highly excited central molecule is assumed. In the condensed phase this exchange is hindered by the high density of solvent molecules, leading to a local heating of the inner solvent shell. This reduction of the temperature difference between the central molecule and its direct surrounding would reduce the energy flow into the solvent. These considerations where taken into account in Ref. 16 by describing the energy exchange between the vibrationally highly excited molecule and the inner solvent shell by isolated binary collisions, and by characterizing the energy transport to the outer solvent as classical heat conduction. The latter process in spherical symmetry is described by the differential equation

$$\frac{\partial(\mathrm{Tr})}{\partial t}=\kappa\,\frac{\partial^2(\mathrm{Tr})}{\partial r^2}\quad\text{with}\quad \kappa=\frac{\lambda}{c_p\rho}. \tag{12}$$

Here, κ, λ, c_p, and ρ are the thermal diffusivity, heat conductivity, specific heat, and density of the solvent, respectively. Representative calculations for this energy transfer model are illustrated in Fig. 18 (for azulene in C_2H_6 at 498 bar and 298 K) and compared with an experimental signal monitored at a probe wavelength of 290 nm (open circles). The simulated signals were obtained by converting calculated $\langle E(t)\rangle$ decays into absorption time profiles using Eqs. (8)–(10). Employing a collision frequency of $Z_D=13.3$ ps^{-1}

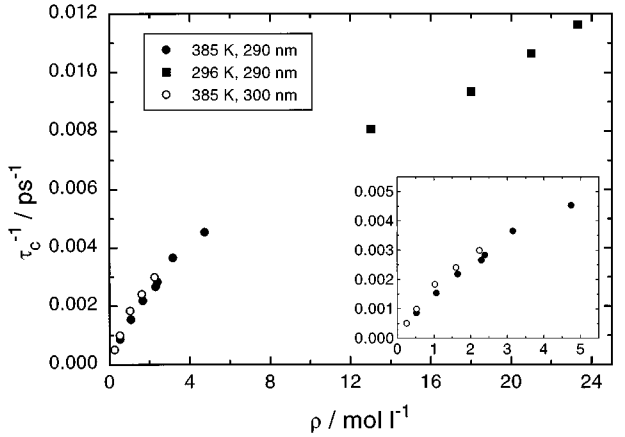

FIG. 10. As Fig. 8, bath gas Xe.

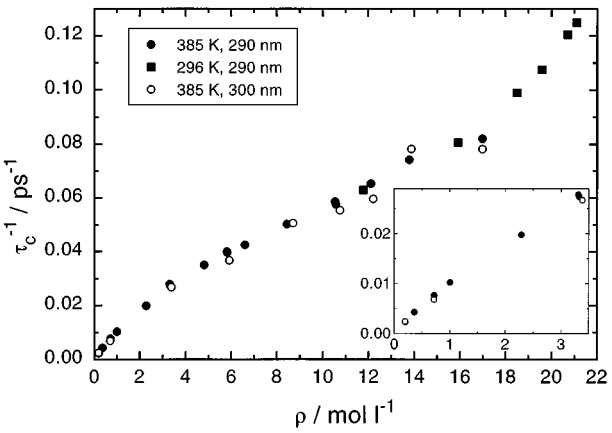

FIG. 12. As Fig. 8, bath gas C_2H_6.

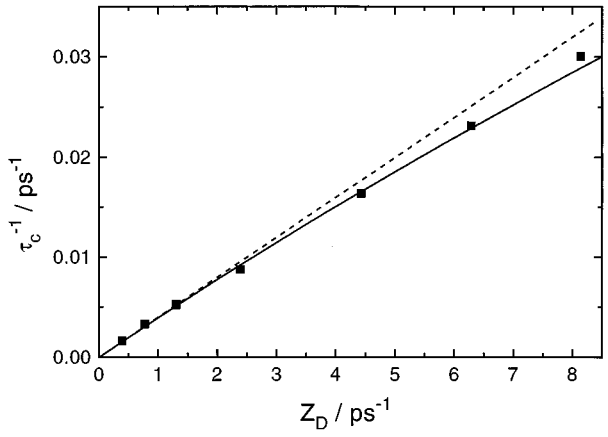

FIG. 13. As Fig. 8, dependence on the collision frequency Z_D, bath gas He [dotted line: extrapolation of low density data; full line: fit using Eq. (16)].

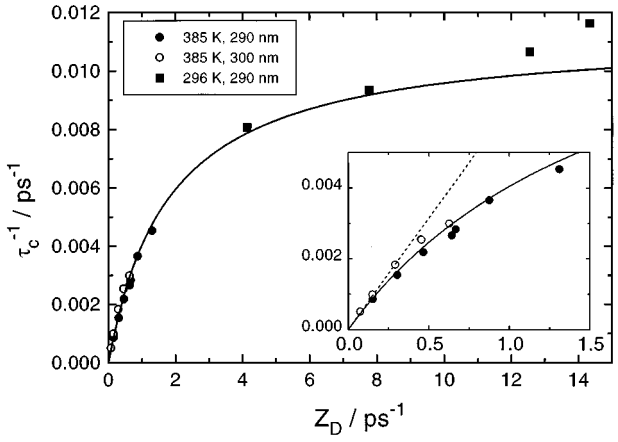

FIG. 15. As Fig. 13, bath gas Xe.

and a linear $\langle \Delta E(E) \rangle$ dependence with the slope found in the gas phase (see Table I), the IBC model without heat conduction predicts a four times faster decay (solid line) than observed experimentally. Accounting for heat conduction such as suggested in Ref. 16, only small deviations from the IBC model are obtained (see dashed line in Fig. 18). For this calculation, we used $c_p = 78.7$ J/mol K,[40] $\lambda = 0.147$ W/mK,[40] and $r_s = 7.0$ Å for the radius of the first solvation shell; in addition we assumed that two C_2H_6 molecules form the first solvation shell. Increasing the number of ethane molecules in the first solvation shell reduces the difference to the IBC model even more, i.e., classical heat conduction is so efficient that no major heating of the inner solvent shell is possible during collisional deactivation (in our case its temperature is always below 450 K). Therefore, as in the simple IBC model, the energy transfer rate is limited by the rate of isolated binary collisions between the central molecule and direct solvent neighbors. In order to simulate signals, which decay on a time scale comparable to our experimental result, λ would have to be reduced at least by a factor of 10 (see dotted line in Fig. 18). However, in contrast to our experimental observation the energy decay then would become highly nonexponential.

Moreover, heat conduction models do not properly describe the leveling off of τ_c^{-1} at higher densities. For azulene in ethane at 385 K, e.g., the deviation from linearity occurs near 30 bar. Under these conditions, the thermal diffusivity κ continuously increases with pressure up to at least 400 bar[40] and would lead to opposite behavior. We, therefore, conclude that heat conduction cannot explain the small collisional deactivation rates observed at high densities.

2. Limitation of energy flow by intramolecular vibrational redistribution

In the dilute gas phase the time between collisions is much longer than the time for reestablishing intramolecular quasiequilibrium of vibrational energy through intramolecular vibrational redistribution (IVR). It is conceivable that IVR at high densities becomes too slow to ensure between collisions the reexcitation of those low frequency vibrational modes which have contributed most to the energy

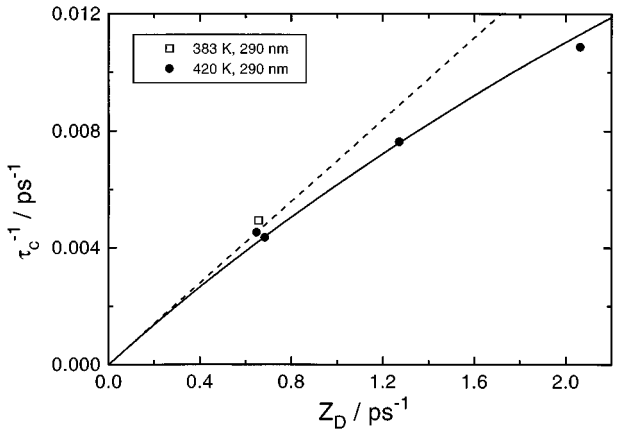

FIG. 14. As Fig. 13, bath gas N_2.

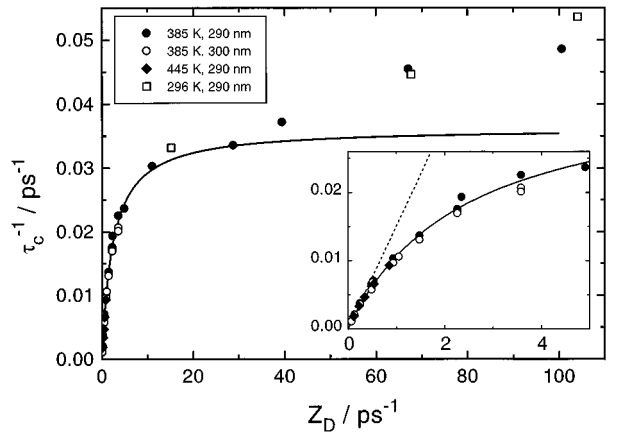

FIG. 16. As Fig. 13, bath gas CO_2.

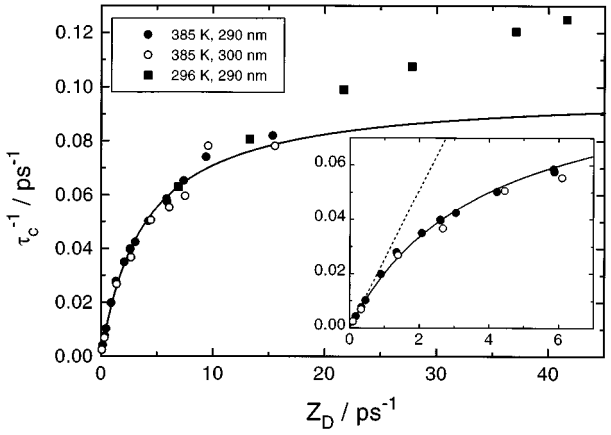

FIG. 17. As Fig. 13, bath gas C_2H_6.

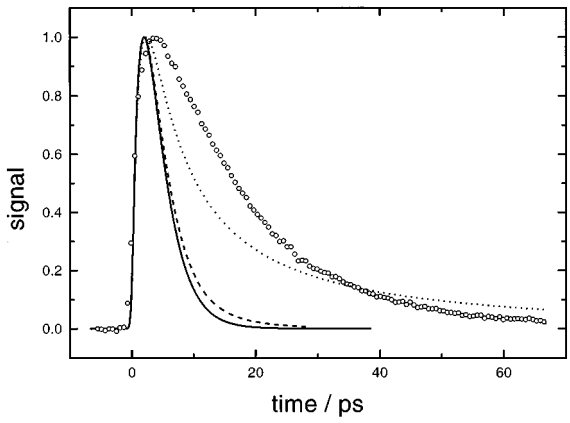

FIG. 18. Simulation of azulene collisional deactivation signals (bath gas C_2H_6, T=296 K, p=498 K; ○: experiment; —: IBC model; ---: IBC model with heat conduction (Ref. 16), $\lambda=\lambda_0=0.147$ W/mK; ⋯ : IBC model with reduced heat conduction, $\lambda=\lambda_0/10$).

transfer.[46,47] Figures 13–17 show that, except for helium, deviations from the extrapolated gas phase behavior of τ_c^{-1} take place at times between collisions of about 3 ps. This is a reasonable time scale for IVR. However, would slow IVR be responsible for the leveling off of τ_c^{-1} at high densities, deviations from the extrapolated gas phase behavior should occur at nearly the same times between collisions in bath gases which transfer approximately equal amounts of energy. Comparing Xe and He this obviously is not the case. Although $m_{\langle\Delta E\rangle}$ decreases by only 30% from Xe to He, the collisional deactivation rate for Xe levels off at $Z_D=0.3$ ps^{-1} whereas for He it does not show any deviations from the dilute gas phase behavior up to $Z_D=6$ ps^{-1}. Our observations, therefore, do not seem to be explicable in terms of an IVR mechanism.

3. Reduction of the collision frequency due to finite lifetimes of collision complexes

Trajectory calculations have shown that collision complexes have lifetimes of several hundreds of femtoseconds.[13,47] One may assume that no energy transfer occurs in a collision of a bath gas molecule with an excited molecule at a site which is just occupied by another collider. In this way, during its life time, a collision complex between azulene and a collider cannot transfer energy as efficiently to the surrounding as uncomplexed azulene. If this picture is correct, the collision frequency of the excited molecule is effectively reduced by a factor of $(1-\theta)$, where $\theta=N/N_{\max}$ is the fractional coverage of the excited molecule by bath gas molecules. Here, N and $N_{\max}$ denote the number of occupied and available sites, respectively. One may try to estimate θ using a simple Langmuir adsorption isotherm model. For adsorption and desorption, one has

$$\frac{dN}{dt}=Z\cdot(1-\theta) \tag{13}$$

and

$$\frac{dN}{dt}=\tau_D^{-1}N_{\max}\theta, \tag{14}$$

respectively, where τ_D is the lifetime of the collision complex. At equilibrium, θ is given by

$$\theta(Z)=\frac{Z}{\tau_D^{-1}\cdot N_{\max}+Z}. \tag{15}$$

Fitting of the model function

$$\tau_c^{-1}(Z_D)=-m_{\langle\Delta E\rangle}\cdot Z_D\cdot(1-\theta(Z_D)) \tag{16}$$

to our experimental data by varying $\tau_D^{-1}\cdot N_{\max}$, leads to good agreement with experimental results up to liquid densities (full lines in Figs. 13–17). The derived values of $\tau_D^{-1}\cdot N_{\max}$ (see last column of Table I) appear quite reasonable considering size and shape of the azulene molecule. For Xe with its large Lennard-Jones diameter and strong interaction potential, e.g., we obtain a value of 1.8 ps^{-1} which is compatible with $N_{\max}=2$ and $\tau_D=1.1$ ps. As expected, the smallest bath gas molecule He with the weakest interaction potential gives the highest value of $\tau_D^{-1}\cdot N_{\max}=65$ ps^{-1}, compatible with $N_{\max}=13$ and $\tau_D=200$ fs. The previous models discussed above, at high densities, all led to nonlinear $\langle\Delta E(E)\rangle$ dependencies and therefore to nonexponential energy decays. Nonlinear $\langle\Delta E(E)\rangle$ dependencies have to be expected also from models which assume that, after laser excitation, existing complexes ''boil off'' adsorbed collider molecules. Latter may transfer momentum to the surrounding bath, creating a cavity which slowly dissipates, leading to a reduction of the energy transfer rate. In contrast to this a reduction of the effective collision frequency ensures that the time dependence of the relaxation remains single exponential over the investigated density range.

So far, in this picture we have only considered the effective collision frequency. Of course, also the average energy transferred per collision can be modified by the formation of collision complexes in dense environments. One may speculate whether the high density deviations from the described model for CO_2 (at $Z_D>30$ ps^{-1}) and for C_2H_6 (at $Z_D>15$ ps^{-1}) are explained by this effect. Obviously, the given

model can only be justified by comparison with extended molecular dynamics simulations. Such investigations are underway in our group.[48]

V. CONCLUSIONS

The present study of collisional energy transfer of highly excited azulene in low pressure gases, supercritical fluids, and compressed liquids has provided reliable information on collisional deactivation rates. The observation over wide density ranges, at first, has shown that isolated binary collision behavior remains valid up to surprisingly high densities. When a certain density is passed, however, a further increase of the energy transfer rate slows down. The observations appear to be of general significance because a parallel study with highly excited cycloheptatriene[45] gave quite similar results. Our discussion has ruled out models with energy transfer bottle-necks by heat conduction or IVR. Instead a reduction of the effective collision frequency through shielding of the excited molecules in complexes led to a surprisingly successful description. These results have to be compared with molecular dynamics simulations.[48]

ACKNOWLEDGMENTS

Discussions of this work with J. Schroeder and K. Luther, as well as financial support by the Deutsche Forschungsgemeinschaft (Sonderforschungsbereich 357 ''Molekulare Mechanismen Unimolekularer Prozesse''), are gratefully acknowledged.

[1] M. Quack and J. Troe, in *Gas Kinetics and Energy Transfer*, edited by P. G. Ashmore and R. J. Donovan, Spec. Per. Rep. (The Chemical Society, London, 1977), Vol. 2, p. 175; H. Hippler and J. Troe, in *Bimolecular Collisions*, edited by M. N. R. Ashfold and J. E. Baggott, Adv. in Gas-Phase Photochem. and Kin. (Royal Society of Chemistry, London, 1989).
[2] D. C. Tardy and B. S. Rabinovitch, Chem. Rev. **77**, 396 (1977); I. Oref and D. C. Tardy, *ibid*. **90**, 1407 (1990).
[3] H. Hippler, J. Troe, and H. J. Wendelken, Chem. Phys. Lett. **84**, 257 (1981); J. Chem. Phys. **78**, 6709 (1983); H. Hippler, K. Luther, and J. Troe, *ibid*. **78**, 6718 (1983); M. Damm, H. Hippler, and J. Troe, *ibid*. **88**, 3564 (1988).
[4] M. Heymann, H. Hippler, D. Nahr, H. J. Plach, and J. Troe, J. Phys. Chem. **92**, 5507 (1988); J. E. Dove, H. Hippler, H. J. Plach, and J. Troe, J. Chem. Phys. **81**, 1209 (1984).
[5] H. Hippler, B. Otto, and J. Troe, Ber. Bunsenges. Phys. Chem. **93**, 428 (1989).
[6] J. Shi, D. Bernfeld, and J. R. Barker, J. Chem. Phys. **88**, 6211 (1988); J. Shi and J. R. Barker, *ibid*. **88**, 6219 (1988).
[7] B. M. Toselli, J. D. Brenner, M. L. Yarram, W. E. Chin, K. D. King, and J. R. Barker, J. Chem. Phys. **95**, 176 (1991).
[8] A. Symonds, Ph.D. thesis, Göttingen, 1992; U. Hold, Ph.D. thesis, Göttingen, 1995; U. Hold, T. Lenzer, K. Luther, and A. Symonds, J. Phys. Chem. (to be published).
[9] J. Troe, J. Chem. Phys. **77**, 3485 (1982); J. R. Barker, J. Phys. Chem. **88**, 11 (1984).
[10] K. F. Lim and R. G. Gilbert, J. Chem. Phys. **80**, 5501 (1984); **84**, 6129 (1986).
[11] A. J. Stace and J. N. Murrell, J. Chem. Phys. **68**, 3028 (1978); N. J. Brown and J. A. Miller, *ibid*. **80**, 5568 (1984): H. Hippler, H. W. Schranz, and J. Troe, *ibid*. **40**, 6158 (1986).
[12] M. Bruehl and G. Schatz, J. Phys. Chem. **42**, 7223 (1988).
[13] Th. Lenzer, K. Luther, J. Troe, R. G. Gilbert, and K. F. Lim, J. Chem. Phys. **103**, 626 (1995).
[14] F. Wondrazek, A. Seilmeier, and W. Kaiser, Chem. Phys. Lett. **104**, 121 (1984).
[15] A. Seilmeier, P. O. J. Scherer, and W. Kaiser, Chem. Phys. Lett. **105**, 140 (1984).
[16] U. Sukowksi, A. Seilmeier, T. Elsaesser, and S. F. Fischer, J. Chem. Phys. **93**, 4094 (1990).
[17] H. Miyasaka, M. Hagihara, T. Okada, and N. Mataga, Chem. Phys. Lett. **188**, 259 (1992).
[18] K. E. Schultz, D. J. Russel, and C. B. Harris, J. Chem. Phys. **97**, 5431 (1992).
[19] R. J. Sension, S. T. Repinec, A. Z. Szarka, and R. M. Hochstrasser, J. Chem. Phys. **98**, 6291 (1993).
[20] K. Lenz, M. Pfeiffer, A. Lau, and T. Elsaesser, Chem. Phys. Lett. **229**, 340 (1994).
[21] T. Elsaesser and W. Kaiser, Ann. Rev. Phys. Chem. **42**, 83 (1991).
[22] B. Otto, J. Schroeder, and J. Troe, J. Chem. Phys. **81**, 202 (1984).
[23] H. Hippler, V. Schubert, and J. Troe, J. Chem. Phys. **81**, 3931 (1984).
[24] G. Maneke, J. Schroeder, J. Troe, and F. Voss, Ber Bunsenges. Phys. Chem. **89**, 896 (1985).
[25] R. Zwanzig, J. Chem. Phys. **34**, 1931 (1969).
[26] D. Schwarzer, J. Troe, and J. Schroeder, Ber. Bunsenges. Phys. Chem. **95**, 933 (1991).
[27] L. Brouwer, H. Hippler, L. Lindemann, and J. Troe, J. Phys. Chem. **89**, 4608 (1985).
[28] Th. Bultmann, D. Bingemann, N. Ernsting, D. Schwarzer, and L. Nikowa, Rev. Sci. Instrum. **66**, 4393 (1995).
[29] M. Heymann, H. Hippler, H. J. Plach, and J. Troe, J. Chem. Phys. **87**, 3867 (1987).
[30] R. S. Chao and R. K. Khanna, Spectrochim Acta, Part A **33**, 53 (1977).
[31] H. Hippler, L. Lindemann, and J. Troe, J. Chem. Phys. **83**, 3906 (1985).
[32] R. Wiebe, V. L. Gaddy, and C. Heins, J. Am. Chem. Soc. **53**, 1721 (1931).
[33] Landolt-Börnstein, *Zahlenwerte und Funktionen*, 6th ed. (Springer, Heidelberg, 1971).
[34] A. Michels, T. Wassenaar, and P. Louwerse, Physica **20**, 99 (1954).
[35] P. W. E. Peerboom, H. Luigjes, and K. O. Prins, Physica A **156**, 260 (1989).
[36] A. Michels, R. J. Lunbeck, and G. J. Wolkers, Physica **17**, 801 (1951).
[37] A. Boushehri, J. Bzowski, J. Kestin, and E. A. Mason, J. Phys. Chem. Ref. Data **16**, 445 (1987).
[38] A. Michels and C. Michels, Proc. R. Soc. London **153**, 201 (1935); **160**, 348 (1937); A. Michels, C. Michels, and H. Wouters, *ibid.* **153**, 214 (1935).
[39] V. V. Altunin, Tr. Mosk. Energ. In-ta **424**, 24 (1979).
[40] D. G. Fried, H. Ingham, and J. F. Ely, J. Phys. Chem. Ref. Data **20**, 274 (1991).
[41] R. C. Reid, J. M. Prausnitz, and T. K. Sherwood, *The Properties of Gases and Liquids*, 3rd ed. (McGraw-Hill, New York, 1977).
[42] A. Greiner-Schmid, S. Wappmann, M. Has, and H.-D. Lüdemann, J. Chem. Phys. **94**, 5643 (1991).
[43] M. Damm, F. Deckert, H. Hippler, and J. Troe, J. Phys. Chem. **95**, 2005 (1991).
[44] K. T. Herzfeld and T. A. Litovitz, *Absorption and Dispersion of Ultrasonic Waves* (Academic, New York, 1959); J. Chesnoy and G. M. Gale, Ann. Phys. (Paris) **9**, 893 (1984).
[45] J. Benzler, S. Linkersdörfer, and K. Luther, Ber. Bunsenges. Phys. Chem. **100**, 1252 (1996).
[46] L. Landau and E. Teller, Physik. Z. Sowjetunion **10**, 34 (1936).
[47] D. C. Clary, R. G. Gilbert, V. Bernshtein, and I. Oref, Faraday Discuss. (to be published).
[48] I. I. Fedchenia, C. Heidelbach, and J. Schroeder, Chem. Phys. Lett. (to be published).